(Received 4 December 2024, Accepted 9 January 2025, Scheduled 22 January 2025)

Direction-of-Arrival Estimation Method of Single Snapshot Coherent Source Based on Hyperbolic Tangent Kernel Correntropy

Hongyuan Gao*, Kailong Liu, and Ying Guo

College of Information and Communication Engineering, Harbin Engineering University, Harbin, China

ABSTRACT: To solve the problem of low accuracy and real-time performance of direction of arrival (DOA) estimation in an impulsive noise environment, this paper proposes a single-snapshot DOA estimation method based on the median deviation correntropy of hyperbolic tangent kerne and designs an intelligent optimization algorithm for the segmentation and hunting mechanism of gold long-nosed raccoon to obtain accurate DOA estimation angle. The DOA estimation method proposed in this paper uses spatial smoothing technology to process the median deviation correntropy of single snapshot data, and then uses the hyperbolic tangent kernel to remove impulse noise from the pseudo-covariance matrix. The weighted signal subspace fitting method is used to obtain the accurate DOA estimation angle. The Monte Carlo analysis experiments of different schemes are verified, especially in the case of a single snapshot, low generalized signal-to-noise ratio (GSNR), and strong impulse noise.

1. INTRODUCTION

The Direction of Arrival (DOA) refers to the direction of arrival of space signals. The main task is to process space signals and estimate their parameters. It has been widely used in many military and civil economic fields such as communication, radar, navigation systems, and radio astronomy [1–3]. It has achieved rapid development in the past 30 years.

Direction of arrival estimation is an important research direction in array signal processing [1]. Its main task is to process space signals and estimate their parameters. It has a wide range of applications in military and civilian fields, such as radar detection [2, 3], electronic countermeasures [4], sonar [5], and wireless sensor networks (WSNs). Subspace-based super-resolution algorithms such as multiple signal classification (MUSIC) algorithm and Estimation of signal parameters via rotational invariance technique (ESPRIT) algorithm usually require the rank of the covariance matrix of the received data to be equal to the number of sources and need more snapshots to obtain the signal subspace and noise subspace to improve the estimation accuracy. They are two common algorithms for DOA estimation. In the process of military confrontation, the signal often appears in a short time and has a fast jump speed. The signal is difficult to be detected, and other scenarios that require the system to have high real-time performance and some physical limitations mean that the number of snapshots used for DOA estimation can only be small, and even in the worst case, there is only a single snapshot.

However, most of the above methods perform DOA estimation in a Gaussian noise environment. In practical applications, there are usually a large number of non-Gaussian noises with peak pulse characteristics, such as sea clutter, ground clutter, atmospheric environment, and radar scattering echoes in nature. It is possible to show bursts and peaks, making the noise environment exhibit strong pulse characteristics [6–8]. In this environment, the performance of conventional DOA methods will seriously degrade or even fail.

There have been some studies on DOA estimation in impulsive noise environment, and the method based on fractional lower order statistics (FLOS) is one of the more effective ones [4, 5]. For example, ROC-MUSIC algorithm based on the common torque is proposed in [6]. Ref. [7] proposes a FLOM-MUSIC algorithm based on fractional lower order moments (FLOM). Ref. [8] proposes a fractional lower order moment cyclic covariance (FLOC) MUSIC algorithm using the FLOC matrix. However, these methods all require prior knowledge of the stable distribution characteristic index, which has certain limitations. By using the characteristics of the kernel function, correlation entropy has a good inhibitory effect on impulse noise and does not require prior knowledge of noise. In this paper, hyperbolic tangent kernel is introduced into the weighted signal subspace fitting algorithm for the first time. The spatial smoothing method is used to process the covariance matrix with the median deviation correntropy, and the hyperbolic tangent kernel median deviation correntropy weighted signal subspace fitting DOA estimation method is proposed.

The Golden Coati optimization algorithm (GCOA) proposed in this paper adopts the golden sine segmentation search strategy [9], introduces the development stage of Harris Eagle Round-Up [10], and finally carries out the crisscross method of disordered dimension sampling, which reduces the computational cost, prevents the reduction of the overall sparsity due

* Corresponding author: Hongyuan Gao (gaohongyuan@hrbeu.edu.cn).

to the reduction of the dimension close to the best individual, and improves the global search ability. Therefore, GCOA can be used to solve the objective function of the median deviation correntropy of the hyperbolic tangent kernel, which is referred to as the Golden Coati weighted signal subspace fitting method based on hyperbolic tangent kernel median deviation correntropy (GCOA-HMCE-WSF) method.

2. SIGNAL AND NOISE MODELS

2.1. Signal Model

It is considered that N narrowband sources are incident on a uniform equidistant linear array composed of Q array elements with θ_i $(i = 1, 2, \ldots N)$. The array element spacing is d, and the wavelength is λ. Taking the first array element as the reference array element, the output of the k-th array element at time t can be expressed as:

$$x_k(t) = \sum_{i=1}^{N} s_i(t) e^{j2\pi \sin\theta_i (k-1)d/\lambda} + n_k(t), \quad (1)$$

$$k = 1, 2, \ldots, Q$$

In the formula, $s_i(t)$ denotes the i-th incident signal; θ_i denotes the direction of arrival; λ denotes the signal's wavelength and satisfies the 'half-wavelength' condition $d \leq \lambda/2$. $n_k(t)$ denotes the additive noise contained in the kth array element. Eq. (1) can be further expressed in the following matrix form:

$$X(t) = AS(t) + N(t) \quad (2)$$

In the formula, the $N \times 1$-dimensional signal vector and $M \times 1$-dimensional noise data vector incident on the array in space can be expressed as:

$$\begin{aligned} S(t) &= [s_1(t), s_2(t), \ldots, s_N(t)]^{\mathrm{T}} \\ N(t) &= [n_1(t), n_2(t), \ldots, n_Q(t)]^{\mathrm{T}} \end{aligned} \quad (3)$$

The $Q \times N$ dimensional manifold matrix (steering vector matrix) $\mathbf{A}$ and the i-th steering vector can be expressed as:

$$A = [a(\theta_2), a(\theta_2), \ldots, a(\theta_N)] \quad (4)$$

where $\mathbf{a}(\theta_i) = [1, e^{j2\pi \sin\theta_i d/\lambda}, \ldots, e^{j2\pi \sin\theta_i (Q-1)d/\lambda}]^{\mathrm{T}}$ is the direction vector of the i-th source.

2.2. Alpha Stable Distribution

The impulse noise in this paper uses the Alpha stable distribution model [11]. Since there is no closed-form probability density function, the Alpha stable distribution is usually characterized by the characteristic function, which is expressed as follows:

$$\Phi(u) = \exp\{ja u - \gamma |u|^{\alpha} [1 + j\beta \mathrm{sgn}(u)\omega(u, \alpha)]\} \quad (5)$$

Among them

$$\mathrm{sgn}(u) = \begin{cases} 1 & u > 0 \\ 0 & u = 0 \\ -1 & u < 0 \end{cases} \quad (6)$$

$$\omega(u, \alpha) = \begin{cases} \tan(\frac{\pi\alpha}{2}), \alpha \neq 1 \\ \frac{2}{\pi} \log|u|, \alpha = 1 \end{cases} \quad (7)$$

It can be seen from formula (3) that the characteristic function is determined by four parameters: α, β, γ, and μ. Parameter α is called characteristic exponent, which is used to measure the tailing thickness of the probability density function, and the value range is $(0, 2]$. When $\alpha = 2$, the stable distribution degenerates into a Gaussian distribution. Parameter β is called the index of skewness, which represents the skewness of the distribution, and the value range is $[-1, 1]$. When $\beta = 0$, the stable distribution is usually called symmetric alpha stable (SαS) distribution. Parameter γ is called scale parameter, which is used to measure the degree of dispersion of the sample. Analogous to the variance of the conventional distribution, the value range is $(0, +\infty)$. Parameter μ is called location parameter, and the value range is $(-\infty, +\infty)$. When $0 < \alpha \leq 1$, μ represents the median of the variable, and when $1 < \alpha \leq 2$, μ represents the mean of the variable.

3. DOA ESTIMATION ALGORITHM BASED ON GCOA-HMCE-WSF

3.1. HMCE-WSF Algorithm

It is assumed that the sources are independent of each other, that the sources and noise are independent of each other, that the mean value of the received data of the array elements is zero, that the received noise between the array elements is uncorrelated, and that the variance is equal. Then, the covariance matrix of the received data can be expressed as:

$$R = E\left[XX^{\mathrm{H}}\right] = AR_S A^{\mathrm{H}} + \sigma_N^2 I \quad (8)$$

$E[\cdot]$ denotes the mathematical expectation, H the conjugate transpose, I the unit matrix, and σ_N^2 the variance of noise.

To make full use of the single snapshot data received by the array, a uniform equidistant linear array of Q elements is divided into M overlapping subarrays by forward sliding. Each subarray has L elements, where $M = Q - L + 1$. Its spatial smoothing structure is shown in Figure 1.

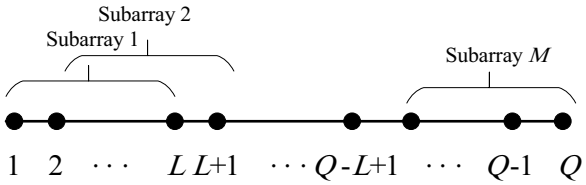

FIGURE 1. Spatial smoothing structure diagram.

Taking the first subarray on the left side as the reference array element, the single snapshot signal received by the mth subarray can be expressed as:

$$\begin{aligned} y_m(t) &= [y_m(t), y_{m+1}(t), \ldots, y_{m+L-1}(t)]^{\mathrm{T}} \\ &= \mathbf{A}(\theta) D(t) \bar{A}_m + n_m(t) \end{aligned} \quad (9)$$

In the formula, $\mathbf{A}(\theta)$ is the corresponding array manifold of the first subarray receiving data. $D(t) = \mathrm{diag}[s_1(t), s_2(t), \ldots, s_N(t)]_{N \times N}$ is the diagonal matrix of the incident signal vector. $n_m(t)$ is the cor-

$$\bar{A}_m = \left[\mathrm{e}^{-\mathrm{j}\frac{2\pi}{\lambda}\sin(\theta_1)(m-1)}, \mathrm{e}^{-\mathrm{j}\frac{2\pi}{\lambda}\sin(\theta_2)(m-1)}, \ldots, \mathrm{e}^{-\mathrm{j}\frac{2\pi}{\lambda}\sin(\theta_N)(m-1)}\right]^{\mathrm{T}}_{N\times 1} \tag{10}$$

The following matrix is constructed by using the data received by M sub-matrices:

$$\mathbf{Y} = \begin{bmatrix} y_1(t) & y_2(t) & \ldots & y_M(t) \\ y_2(t) & y_3(t) & \ldots & y_{M+1}(t) \\ \vdots & \vdots & \ddots & \vdots \\ y_L(t) & y_{L+1}(t) & \ldots & y_Q(t) \end{bmatrix}_{L\times M} \tag{11}$$

According to Eq. (10), matrix Y can be expressed as:

$$Y = A(\theta)D(t)\bar{A} + n(t) \tag{12}$$

where $\bar{A}$ can be specifically expressed as:

$$\begin{aligned} \bar{A} &= \left[\bar{A}_1, \bar{A}_2, \ldots, \bar{A}_{M-1}\right] \\ &= \begin{bmatrix} 1 & \mathrm{e}^{-\mathrm{j}\frac{2\pi}{\lambda}\sin(\theta_1)} & \ldots & \mathrm{e}^{-\mathrm{j}\frac{2\pi}{\lambda}\sin(\theta_1)(M-1)} \\ 1 & \mathrm{e}^{-\mathrm{j}\frac{2\pi}{\lambda}\sin(\theta_2)} & \ldots & \mathrm{e}^{-\mathrm{j}\frac{2\pi}{\lambda}\sin(\theta_2)(M-1)} \\ \vdots & \vdots & \ddots & \vdots \\ 1 & \mathrm{e}^{-\mathrm{j}\frac{2\pi}{\lambda}\sin(\theta_N)} & \ldots & \mathrm{e}^{-\mathrm{j}\frac{2\pi}{\lambda}\sin(\theta_N)(M-1)} \end{bmatrix}_{N\times M} \end{aligned} \tag{13}$$

The noise vector matrix is:

$$n(t) = \begin{bmatrix} n_1(t) & n_2(t) & \ldots & n_M(t) \\ n_2(t) & n_3(t) & \ldots & n_{M+1}(t) \\ \vdots & \vdots & \ddots & \vdots \\ n_L(t) & n_{L+1}(t) & \ldots & n_Q(t) \end{bmatrix}_{L\times M} \tag{14}$$

To reduce the influence of noise and enable it to realize feature decomposition, covariance processing is performed on the constructed matrix Y:

$$R_y = YY^{\mathrm{H}} = A(\theta)D(t)\bar{A}\bar{A}^{\mathrm{H}}D(t)^{\mathrm{H}}A(\theta)^{\mathrm{H}} + \sigma^2 I \tag{15}$$

The matrix after covariance processing has the conjugate symmetry property, but the diagonal elements do not match. Therefore, to construct the Toeplitz matrix, the diagonal elements are median processed to obtain the following matrix:

$$\mathbf{R}_y = \begin{bmatrix} \tilde{y}_1(1) & \tilde{y}_2^*(1) & \ldots & \tilde{y}_L^*(1) \\ \tilde{y}_2(1) & \tilde{y}_1(1) & \ldots & \tilde{y}_{L-1}^*(1) \\ \vdots & \vdots & \ddots & \vdots \\ \tilde{y}_L(1) & \tilde{y}_{L-1}(1) & \ldots & \tilde{y}_1(1) \end{bmatrix}_{L\times L} \tag{16}$$

To obtain a better estimation effect in the impact noise environment, the low-order moment matrix based on the hyperbolic tangent kernel correlation entropy is obtained by processing Eq. (15) and Eq. (16) and using the hyperbolic tangent kernel median deviation correlation entropy:

$$\mathbf{R} = \begin{bmatrix} \tilde{r}_{11} & \tilde{r}_{12} & \ldots & \tilde{r}_{1L} \\ \tilde{r}_{21} & \tilde{r}_{22} & \ldots & \tilde{r}_{2L} \\ \vdots & \vdots & \ddots & \vdots \\ \tilde{r}_{L1} & \tilde{r}_{L2} & \ldots & \tilde{r}_{LL} \end{bmatrix}_{L\times L} \tag{17}$$

where the specific elements can be expressed as

$$\tilde{r}_{ij} = \frac{1}{L}\sum_{k=1}^{L}\begin{pmatrix} (R_y(i,k) - \tilde{y}(i,k)) \cdot (R_y(j,k) \\ -\tilde{y}(j,k))^* \cdot \tanh(\frac{\mathbf{R}_y(:,k)\cdot(\mathbf{R}_y(:,k))^{\mathrm{H}}}{2\sigma^2}) \end{pmatrix} \tag{18}$$

where $\tilde{r}_{ij}$ represents each element in the matrix $\mathbf{R}$. $\tanh(\cdot)$ is the kernel function of the hyperbolic tangent kernel, σ the kernel length of the kernel function, $R_y(i,k)$ the element of row i and column k in matrix $\mathbf{R}_y$, $(\cdot)^*$ the conjugate, and $(\cdot)^H$ the conjugate transpose.

The characteristic decomposition of $\tilde{R}$ can be obtained:

$$\tilde{R} = U_s V_s U_s^{\mathrm{H}} + U_n V_n U_n^{\mathrm{H}} \tag{19}$$

U_s represents the signal subspace spanned by the eigenvector corresponding to the large eigenvalue, U_n the noise subspace spanned by the eigenvector corresponding to the small eigenvalue, V_s a diagonal matrix composed of N large eigenvalues, and V_n a diagonal matrix composed of small eigenvalues. The orthogonal projection matrix is:

$$\mathbf{P}_{\mathbf{A}(\theta)} = \mathbf{A}(\theta)\left(\mathbf{A}^{\mathrm{H}}(\theta)\mathbf{A}(\theta)\right)^{-1}\mathbf{A}^{\mathbf{H}}(\theta) \tag{20}$$

The angle estimation equation of the single-snapshot weighted signal subspace fitting equation based on the hyperbolic tangent kernel median deviation correntropy is:

$$\hat{\theta} = \arg\max_{\theta} \mathrm{tr}\left\{\mathbf{P}_{\mathbf{A}(\theta)} U_s W U_s^{\mathrm{H}}\right\} \tag{21}$$

In the formula $W = (V_s - \mu I)^2 V_s^{-1}$, μ is the average of $L-N$ small eigenvalues, $\mathbf{I}$ the unit matrix, and $\mathrm{tr}(\cdot)$ the matrix trace function.

In this case, the pseudo-covariance matrix of the mean deviation correntropy of the hyperbolic tangent kernel can be used to obtain the estimated value of the WSF algorithm under impulse noise. The proposed single-snapshot estimation method based on the HMCE-WSF applicable to Gaussian noise, Cauchy noise, weak impulse noise, and strong impulse noise. In addition, the HMCE-WSF method proposed in this paper is suitable not only for uniform linear arrays (ULA), but also for uniform circular arrays (UCA), planar arrays, special arrays, and other complex array structures.

3.2. GCOA Algorithm

The Coati Optimization Algorithm simulates two natural behaviors of coati in nature [12]: (a) the behavior of attacking and hunting iguanas and (b) the behavior of fleeing from predators. In this paper, the golden sine strategy is integrated into the exploration stage of COA to enhance the algorithm's global search ability. To solve the problems of uneven population distribution, reduced diversity, and low population quality in the initial stage of the traditional COA algorithm, this paper uses a good point set and a dynamic reverse learning strategy to initialize the population to further increase the diversity of the algorithm

population and the number of population elite individuals to help the algorithm expand the search area. The development of a traditional COA algorithm lacks the guidance of the best information, which may not be conducive to rapid convergence in the later stage. In this paper, the soft and hard encirclements and fast dive strategy of Harris Hawk algorithm (HHO) are introduced in the development stage. The soft encirclement or hard encirclement is selected by prey energy, and the Levy walk or fast dive attack is judged according to the fitness, so that the algorithm can effectively jump out of the local optimum. In addition, in the later iteration of the GCOA algorithm, to improve the calculation accuracy of the algorithm and the ability to jump out of the local optimum, the disordered dimension vertical and horizontal crossover strategy [13] is used to modify the individual, and the horizontal crossover is used to cross-search the population to reduce the search blind spot. The vertical crossover increases the population diversity and reduces the probability of the algorithm falling into the local optimum.

Suppose that we need to solve the maximum value of the function $f(\tilde{h}_{\bar{k}}(\bar{i})), \tilde{h}_{\bar{k}}(\bar{i}) \in R_M$, where R_M is a real M-dimensional space and $\tilde{h}_{\bar{k}}(\bar{i}) = [\tilde{h}_{\bar{k},1}(\bar{i}), \tilde{h}_{\bar{k},2}(\bar{i}), \ldots, \tilde{h}_{\bar{k},M}(\bar{i})]$.

Firstly, the GCOA algorithm is set as follows: the number of golden coati is set to C_P; the search space dimension of each long-nosed raccoon is M; the maximum number of iterations is G; and the current number of iterations is g. The location of the g-th generation of the $\bar{i}$ raccoon is defined as $h_{\bar{i}}^g = [h_{\bar{i},1}^g, h_{\bar{i},2}^g, \ldots, h_{\bar{i},M}^g]$. The position of the optimal raccoon individual in the g-th generation is $h_{\text{best}}^g = [h_1^g, h_2^g, \ldots, h_M^g]$, and $\bar{h}_{\bar{I}}^g = [\bar{h}_{\bar{I},1}^g, \bar{h}_{\bar{I},2}^g, \ldots, \bar{h}_{\bar{I},M}^g]$ denotes the new position of the iguana on the ground. *Sp* is the escape probability of prey, which is a random number between $(0, 1)$; $|E|$ is the escape energy of prey, which is defined as $E = 2\text{rand} \cdot (1 - \frac{g}{G})$; rand represents a random number between $(0, 1)$.

Through the initialization of the good point set, C_P population $\tilde{\mathbf{h}}$ is generated. Through the following formula, the dynamic reverse learning strategy is carried out on the population after the initialization of the point set:

$$\mathbf{h} = \tilde{\mathbf{h}} + \tilde{r}_1 \times \left(\tilde{r}_1 \times \left(l_b + u_b - \tilde{\mathbf{h}}\right) - \tilde{\mathbf{h}}\right) \tag{22}$$

In the search space, the first stage is the exploration stage: a group of coati climb up a tree and use the golden sine segmentation search method to approach the iguana and expel it. Other coati wait under the tree until the iguana falls to the ground. After the iguana lands, the long-nosed raccoon will attack it and hunt it.

In the exploration stage, the long-nosed raccoon uses the golden sine segmentation strategy to search for the iguana. The search formula is as follows:

$$\begin{aligned} h_{\bar{i}}^{g+1}(m) &= w_g \cdot h_{\bar{i}}^g(m) \cdot |\sin R_1| \\ &\quad + r_1 \sin(2r_2) \cdot \left(t_1 h_{\text{best}}^g(m) - t_2 \cdot I_1 \cdot h_{\bar{i}}^g(m)\right) \end{aligned} \tag{23}$$

where $\bar{i} = 1, 2, \ldots, C_p/2$, $w_g = 0.3 + 0.6\frac{g}{G}$, $R_1 = 2\pi \cdot \text{rand}$, $r_1, r_2 = \pi \cdot \text{rand}$, I_1 denotes a random integer in the set of integers {1,2}, $t_1 = -\pi + \frac{1-(\sqrt{5}-1)/2}{2\pi}$, $t_2 = -\pi + (\sqrt{5}-1) \cdot 2\pi$.

After the iguana falls to the ground, it is placed in a random position in the search space. Based on this random position, the gold long-nosed raccoon on the ground moves in the search space and updates the position using Formulas (24) and (25).

$$\begin{aligned} & h_{\bar{i}}^{g+1}(m) \\ = \; & w_g \cdot h_{\bar{i}}^g(m) \cdot |\sin R_2| \\ & + r_3 \sin(2r_4) \cdot \left| t_1 \bar{h}_{\bar{I},m}^g - t_2 \cdot I_2 \cdot h_{\bar{i}}^g(m) \right|, f(h_{\bar{i}}^g(m)) \\ & < f\left(\bar{h}_{\bar{I},m}^g\right) \end{aligned} \tag{24}$$

$$\begin{aligned} & h_{\bar{i}}^{g+1}(m) \\ = \; & w_g \cdot h_{\bar{i}}^g(m) \cdot |\sin R_2| \\ & + r_3 \sin(2r_4) \cdot \left| t_1 h_{\bar{i}}^g(m) - t_2 \bar{h}_{\bar{I},m}^g \right|, f(h_{\bar{i}}^g(m)) \\ & \geq f\left(\bar{h}_{\bar{I},m}^g\right), \end{aligned} \tag{25}$$

where $i = \frac{C_p}{2} + 1, \frac{C_p}{2} + 2, \ldots, C_p$, $R_2 = 2\pi \cdot \text{rand}$, $r_3, r_4 = \pi \cdot \text{rand}$, I_2 denotes a random integer in the set of integers $\{1, 2\}$.

If the new position calculated by each gold long-nosed raccoon improves the value of the objective function, the new position is acceptable; otherwise, the gold long-nosed raccoon remains in the previous position.

The second stage, the stage of coati escaping from predators, is also called development stage. In this stage, the soft and hard encirclements and fast dive strategies of the Harris eagle are introduced. The soft encirclement or hard encirclement is selected by prey energy, and Levi's walk or fast dive attack is judged according to the fitness, so that the algorithm can effectively jump out of the local optimum.

When $0.5 \leq |E| < 1$ and $Sp \geq 0.5$, the soft encirclement strategy is adopted, and the update formula is:

$$\begin{aligned} h_{\bar{i}}^{g+1}(m) &= \left(h_{\text{best}}^g(m) - h_{\bar{i}}^g(m)\right) \\ &\quad - E \cdot \left| J_{u_1} \cdot h_{\text{best}}^g(m) - h_{\bar{i}}^g(m) \right| \end{aligned} \tag{26}$$

where $J_u = 2 \cdot (1 - \text{rand})$.

When $|E| < 0.5|$ and $Sp \geq 0.5$, the hard-surround strategy is adopted, and the update formula is:

$$h_{\bar{i}}^{g+1}(m) = h_{\text{best}}^g(m) - E \cdot \left| h_{\text{best}}^g(m) - h_{\bar{i}}^g(m) \right| \tag{27}$$

When $0.5 \leq |E| < 1$ and $Sp < 0.5$, the progressive fast subduction soft encirclement strategy is adopted, and the position and direction of the prey are gradually corrected according to the deceptive behavior of the prey, so as to select the best position to capture the prey. It is implemented through the following two strategies. When the first strategy is invalid, the second strategy is executed, and the update formulas are:

$$h_{\bar{i}}^{g+1} = h_{\text{best}}^g - E \cdot \left| J_{u_2} \cdot h_{\text{best}}^g - h_{\bar{i}}^g \right| \tag{28}$$

$$h_{\bar{i}}^{g+1} = h_{\text{best}}^g - E \cdot \left| J_{u_2} \cdot h_{\text{best}}^g - h_{\bar{i}}^g \right| + r_5 \, \text{Levy} \tag{29}$$

In the formula, r_5 is a random number between $(0, 1)$; Levy is Levy's flight strategy; and the formula is:

$$Levy = 0.01 \frac{u \cdot \tilde{\sigma}}{|v|^{\frac{1}{\tilde{\beta}}}}, \quad \tilde{\sigma} = \left(\frac{\Gamma(1+\tilde{\beta}) \cdot \sin(\frac{\pi\tilde{\beta}}{2})}{2^{\left(\frac{\tilde{\beta}-1}{2}\right)} \cdot \Gamma(\frac{1+\tilde{\beta}}{2}) \cdot \tilde{\beta}} \right) \tag{30}$$

where $\beta = 1.5$, u, v are random numbers obeying $(0, 1)$ standard normal distribution, and r_6 is random number between $(0, 1)$.

When $|E| < 0.5$ and $Sp < 0.5$, the Harris hawks try to shorten the distance between them and the average position of the target prey by using the progressive rapid subduction hard encirclement. The update position formula of this strategy of hawk is similar to the formula in the soft encirclement of the progressive rapid subduction. When the first strategy is invalid, the second strategy is executed, and the update formulas are respectively:

$$h_{\tilde{i}}^{g+1} = h_{\text{best}}^{g} - E \cdot \left| J_{u_3} \cdot h_{\text{best}}^{g} - h_{\text{mean}}^{g} \right|, \tag{31}$$

$$h_{\tilde{i}}^{g+1} = h_{\text{best}}^{g} - E \cdot \left| J_{u_4} \cdot h_{\text{best}}^{g} - h_{\text{mean}}^{g} \right| + r_6 Levyv \tag{32}$$

where h_{mean}^{g} is the average position of the g-th golden coati, and r_6 is a random number between $(0, 1)$.

Horizontal crossover refers to selecting two individuals from the same dimension of the population, exchanging individual information according to a certain random proportion, generating their own offspring, and updating the position of the individual through the survival of the fittest to improve the global optimization performance of the algorithm. The expression is:

$$\begin{aligned} Y_{\tilde{j}}^{g+1}(m) &= q_2 \cdot h_{\tilde{j}}^{g}(m) + (1 - q_2) \cdot h_{\tilde{i}}^{g}(m) \\ &\quad + c_2 \cdot \left(h_{\tilde{j}}^{g}(m) - h_{\tilde{i}}^{g}(m) \right) \end{aligned} \tag{33}$$

$$\begin{aligned} Y_{\tilde{i}}^{g+1}(m) &= q_1 \cdot h_{\tilde{i}}^{g}(m) + (1 - q_1) \cdot h_{\tilde{j}}^{g}(m) \\ &\quad + c_1 \cdot \left(h_{\tilde{i}}^{g}(m) - h_{\tilde{j}}^{g}(m) \right) \end{aligned} \tag{34}$$

where $Y_{\tilde{i}}^{g+1}(m)$ and $Y_{\tilde{j}}^{g+1}(m)$ are the m-th dimension of the offspring individuals i and j obtained after crossing. $h_{\tilde{i}}^{g}(m)$ and $h_{\tilde{j}}^{g}(m)$ are the m-th dimension of the parent individuals i and j. q_1 and q_2 are random numbers between $[0, 1]$. c_1 and c_2 are random numbers between $[-1, 1]$. The number of cross dimensions is determined by the sampling rate, which is defined as:

$$\text{Rate}_{\text{sample}} = \text{ceil}\left(\max\left(\frac{g}{G}, \varepsilon_1 \right) \times \text{dim} \right) \tag{35}$$

where $\text{Rate}_{\text{sample}}$ is the sampling rate, $\text{ceil}(\cdot)$ the rounding operator, ε_1 the minimum sampling number, which can avoid the early lower sampling rate, and dim is the dimension.

Vertical crossover refers to the exchange of dimensional information between different dimensions of the best individuals in the population according to a certain vertical crossover probability, thus generating a new generation of the best individuals to compete with their parents, which is conducive to learning from each other in different dimensions and avoiding premature convergence of a certain dimension. The expression is:

$$Y_{best}^{g+1}(m) = q \cdot h_{best}^{g}(m) + (1 - q) \cdot h_{best}^{g}(\bar{m}) \tag{36}$$

where q is a random number between $[0, 1]$, and $Y_{best}^{g+1}(m)$ is the offspring obtained after the parent generation crosses. Similarly, the cross-dimension is determined by the sampling rate.

In the process of repeated iteration, the position of the golden coati with the largest fitness value is selected as the global optimal position. When the maximum number of iterations G is reached, the global optimal position of the golden coati h_{best}^{G} is taken as the optimal solution output of the solution function $f(h_{best}^{G})$.

3.3. GCOA-HMCE-WSF Method for DOA Estimation

For the direction-finding problem of HMCE-WSF in impulsive noise environment, the position of the golden coati represents a potential solution in the direction-finding equation of WSF. In the maximum optimization problem of HMCE-WSF, the estimated parameter θ represents the position of the golden coati, which corresponds to the GCOA algorithm. The fitness value is expressed as:

$$f_{\tilde{i}}^{g} = f(\tilde{\mathbf{h}}_{\tilde{i}}^{g}) = \text{tr}\left[\mathbf{P}_{\mathbf{A}(\theta)} U_s W U_s^{\text{H}} \right] \tag{37}$$

The fitness value is used to evaluate the state of each golden coati. In the DOA estimation problem, the purpose is to search the population position corresponding to the maximum fitness value. The global optimal golden coati is equivalent to the optimal direction vector $\hat{\theta}$, so the DOA estimation problem is transformed into a continuous optimization problem for searching for the optimal position.

In summary, GCOA-HMCE-WSF can be described by the following steps:

(a) Receive the single snapshot data sent by the array antenna $y(t)$.

(b) The received data of each subarray is obtained by forward sliding: $y_1(t), y_2(t), \ldots, y_M(t)$.

(c) Matrix Y is constructed according to Formula (11), and matrix $\mathbf{R}_y$ is obtained by pseudo-covariance median deviation processing.

(d) According to Formula (18), the matrix $\mathbf{R}_y$ is processed by hyperbolic tangent kernel correntropy to obtain matrix $\mathbf{R}$.

(e) The orthogonal projection matrix is obtained by eigendecomposition of $\mathbf{R}$, and the HMCE-WSF angle estimation equation is constructed. According to Formula (37), it is transformed into the maximum value to optimize the fitness function.

(f) The golden raccoon optimization algorithm population is initialized by using the good point set and dynamic reverse learning strategy, and the fitness value is calculated to determine the location of the iguana.

(g) Exploration stage: the golden sine segmentation strategy is used to hunt the iguana and update the population position.

(h) Development stage: using Harris Hawk soft, hard surrounded, rapid subduction strategy to update the population.

(i) The vertical and horizontal crossover strategy uses disordered dimension sampling

(j) To determine whether the maximum number of iterations G is reached, if not, return step (g); if it is reached, the iteration is terminated, and the global optimal gold raccoon position is output as the direction of arrival estimation result output.

The implementation of the proposed method is shown in Algorithm 1.

Algorithm 1 the Proposed Method

Input: Single snapshot data received in impulsive noise environment

Output: Single snapshot DOA estimation angle value

1: Construct $\mathbf{R}_y$ as (16), And according to Formula (18), the formula is processed to obtain Formula (17) $\mathbf{R}$.

2: Pair (17) Eigen-decomposition formula (19).

3: According to formula (19) and formula (20), the angle estimation Equation (21) is obtained.

4. The formula (21) is transformed into the fitness function formula (37).

5. The GCOA algorithm is used to optimize the maximum value of Equation (37) to obtain the DOA estimation angle.

4. SIMULATION RESULTS AND DISCUSSION

4.1. Performance Test of the GCOA-HMCE-WSF Algorithm

To verify the performance of the GCOA-HMCE-WSF algorithm proposed in this paper, a series of simulation experiments and related analyses will be carried out in this section.

Assuming that the number of array elements is 64, the number of sub-arrays is 16, and four completely coherent far-field narrowband signals are used as the incident sources. Their DOA incident directions are $\theta_1 = -45^\circ$, $\theta_2 = -10^\circ$, $\theta_3 = 30^\circ$, $\theta_2 = 60^\circ$, respectively. The number of snapshots is set to 1, and the interference noise is modeled by the Alpha stable distribution model. Since there is no finite second-order moment in the stable distribution noise, the generalized signal-to-noise ratio (GSNR) [14] is used to measure the intensity of impulse noise, which is defined as:

$$\mathrm{GSNR} = 10\log_{10}\frac{P_{\mathrm{s}}}{\gamma} \tag{38}$$

where P_{s} denotes the signal power, and γ denotes the dispersion coefficient of Alpha stable distribution.

The parameters of GCOA algorithm are set as follows: the number of population is $C_p = 100$, and the maximum number of iterations is $G = 2000$.

In the simulation experiment, different experimental conditions are set to evaluate the performance of the algorithm, and 1000 independent Monte Carlo experiments are carried out for each condition. The five comparison algorithms are One-bit-AN [15], 1-D estimation based on particle swarm optimization (1D-PSO-MUSIC [16]), SSCS-MUSIC [17], MPDNN [18], FLOM-ML [19], and CRB. To quantitatively analyze the performance of each algorithm, this paper uses two indicators as evaluation criteria, namely, estimation accuracy and root mean square error (RMSE).

Assuming that the angle of N sources incident on the array is $\theta = [\theta_1, \theta_2, \ldots, \theta_N]$, the corresponding DOA estimation is $\hat{\theta} = [\hat{\theta}_1, \hat{\theta}_2, \ldots, \hat{\theta}_N]$. The number of Monte Carlo experiments is $\tilde{Q}$, and the definition of the estimation accuracy is as follows:

$$P_{\mathrm{Acc}} = \frac{N_{\mathrm{Acc}}}{N_{\mathrm{Tol}}} \tag{39}$$

In the formula, N_{Tol} denotes the total number of experiments, and N_{Acc} denotes the total number of experiments which denotes the number of correct DOA estimations. A correct DOA estimation needs to satisfy the condition. $|\hat{\theta}_i(k) - \theta_i| \leq 1^\circ$. Among them, $\hat{\theta}_i(k)$ represents the DOA estimation of the i-th source in the k-th experiment, and θ_i represents the true DOA estimation of the i-th source. The corresponding root mean square error (RMSE) is defined as follows:

$$\mathrm{RMSE} = \sqrt{\frac{1}{\tilde{Q}N}\sum_{i=1}^{\tilde{Q}}\sum_{k=1}^{N}\left|\hat{\theta}_k(i) - \theta_k\right|^2} \tag{40}$$

4.2. The Simulation Results of the Algorithm under Different Characteristic Indexes

This group of experiments analyzes the influence of the characteristic index on the performance of the algorithm. The smaller the characteristic index is, the stronger the impulse of the noise is, GSNR = 1 dB. The number of snapshots is 1, and the performance of the algorithm is shown in Figure 2 and Figure 3. It can be seen from the graph that One-bit-AN has the worst performance in an impulse noise environment, and as the characteristic index decreases, the performance decays fastest, and its resistance to impulse noise is the worst. Due to the low number of snapshots set in the experiment, the performance of MPDNN and FLOM-ML algorithms also decays rapidly. The above four algorithms almost fail in the robust pulse environment below $\alpha = 1$. The performance of GCOA-HMCE-WSF algorithm in this paper is significantly better than the other five comparison algorithms, and it still has better estimation performance in a strong impulse noise environment.

4.3. The Effect of GSNR on the Performance of the Algorithm

This group of experiments analyzes the effect of GSNR on the algorithm's performance. In the stable distributed noise environment with 5 snapshots and $\alpha = 1.5$, the impact of GSNR on the performance of the algorithm is shown in Figure 4 and Figure 5. It can be seen from the graph that One-bit-AN and 1D-pso-MUSIC perform well when the GSNR is high, but the performance of the algorithm decreases significantly as the GSNR decreases. FLOM-ML and MPDNN algorithms perform well when GSNR is high. However, when GSNR is less than 0 dB, the performance of these algorithms decreases significantly. The algorithm GCOA-HMCE-WSF in this paper performs better than the other five comparison algorithms in the case of each GSNR.

4.4. The Influence of Source Spacing on DOA Estimation

This group of experiments analyzes the influence of the DOA interval of two sources on the algorithm's performance, as

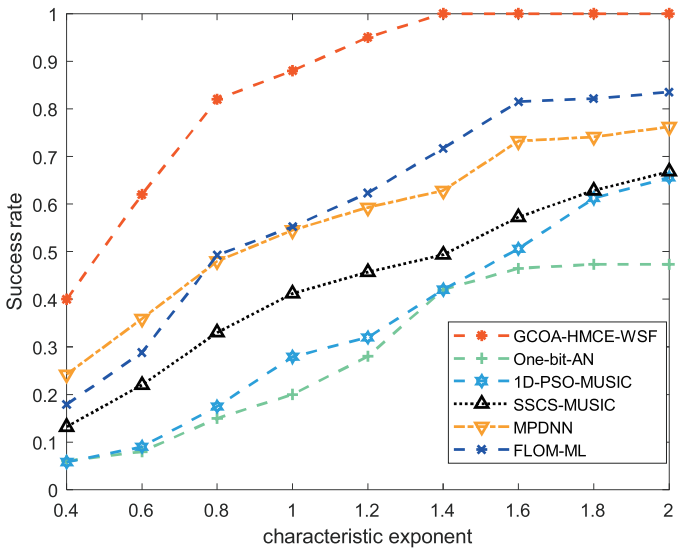

FIGURE 2. The success rate simulation comparison curves under different characteristic indexes.

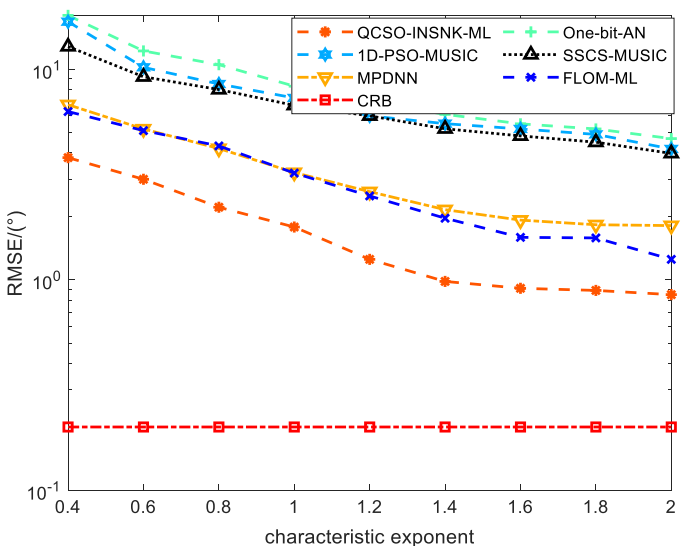

FIGURE 3. RMSE simulation comparison curve under different characteristic indexes.

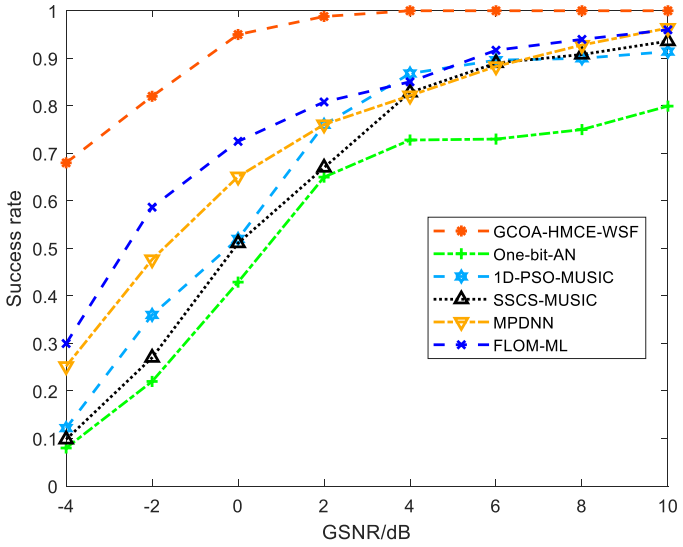

FIGURE 4. The success rate simulation comparison curves under different GSNRs.

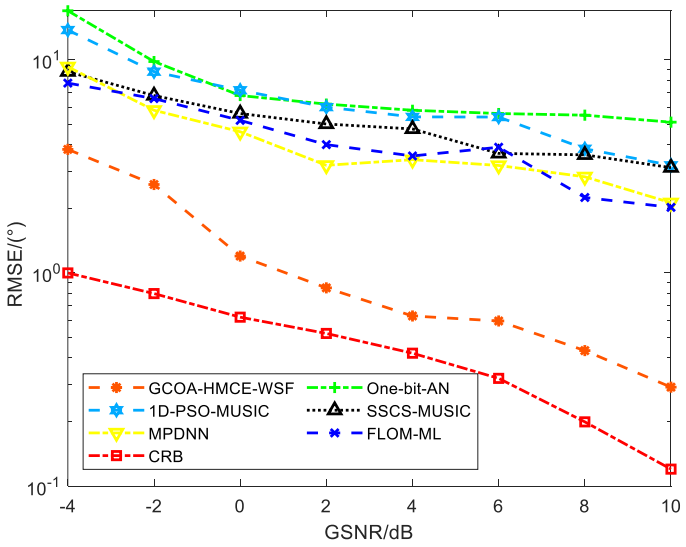

FIGURE 5. RMSE simulation comparison curves under different GSNRs.

shown in Figure 6 and Figure 7. The DOA of source 1 is fixed as $\theta = 10°$; the angle θ of source 2 is in the range of $[11, 20]$; the impact strength $\alpha = 1$, GSNR $= 10$ dB. When the DOA interval is less than a particular value, the correct DOA value cannot be estimated, and the algorithm is almost ineffective. It can be seen from the graph that the minimum resolution success angle interval of One-bit-AN and 1D-PSO-MUSIC algorithms is the largest. SSCS-MUSIC, MPDNN, and FLOM-ML have smaller minimum resolution success angle intervals. The GCOA-HMCE-WSF algorithm in this paper has the best effect, and the minimum resolution success angle interval is 2°. At the same time, as the DOA interval of the source becomes smaller, the performance of each algorithm decreases. In contrast, the performance of the DMCE-MUSIC algorithm is better than the other five comparison algorithms, and the gap with the Cramer-Rao bound is smaller, showing a broader applicability.

4.5. Performance Analysis of DOA Estimation for Coherent Signals

This group of experiments analyzes the influence of two coherent signals on the algorithm's performance, as shown in Figure 8 and Figure 9. The incident angles of coherent sources 1 and 2 are $\theta_1 = 10°$ and $\theta_2 = 30°$, characteristic exponent $\alpha = 1.5$ and GSNR $= 10$ dB. It can be seen from the figure that the low-order moment direction-finding methods based on the MUSIC algorithm class cannot achieve accurate estimation of coherent sources. In contrast, the FLOM-ML and GCOA-HMCE-WSF algorithms have a high success rate for coherent source estimation. Among them, the algorithm proposed in this paper has better performance.

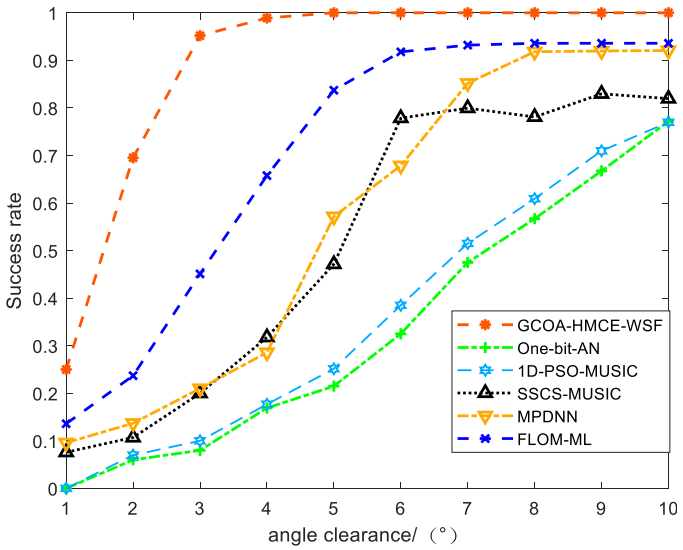

FIGURE 6. The success rate simulation comparison curve under different angle intervals.

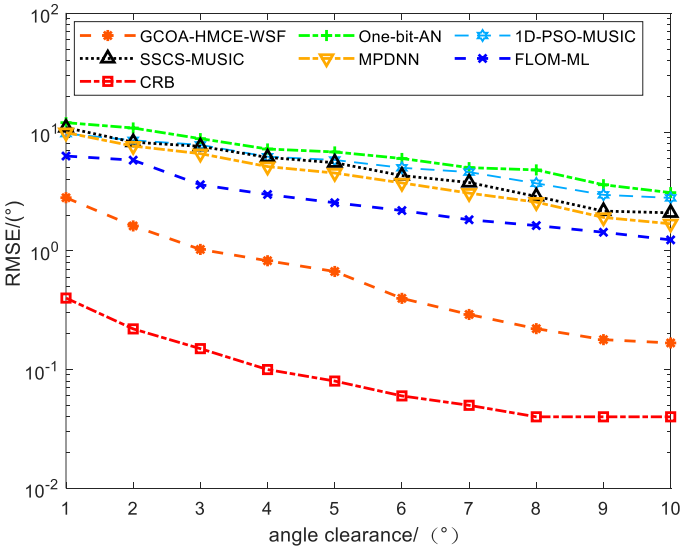

FIGURE 7. RMSE simulation comparison curves at different angle intervals.

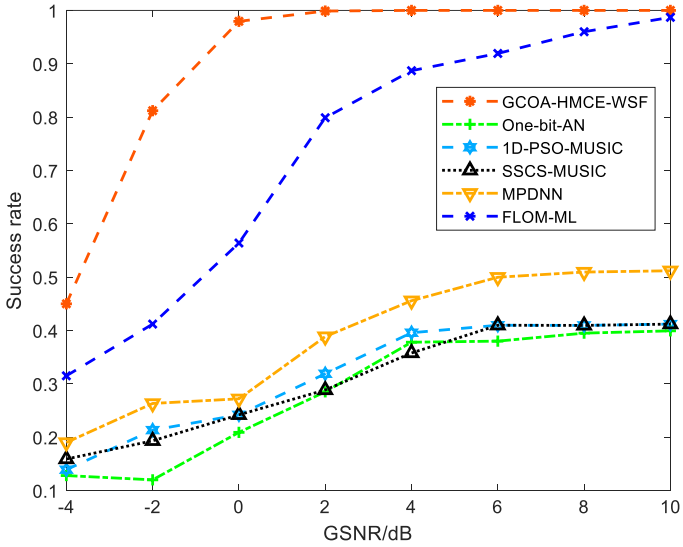

FIGURE 8. The success rate simulation curves of two coherent sources under different GSNRs.

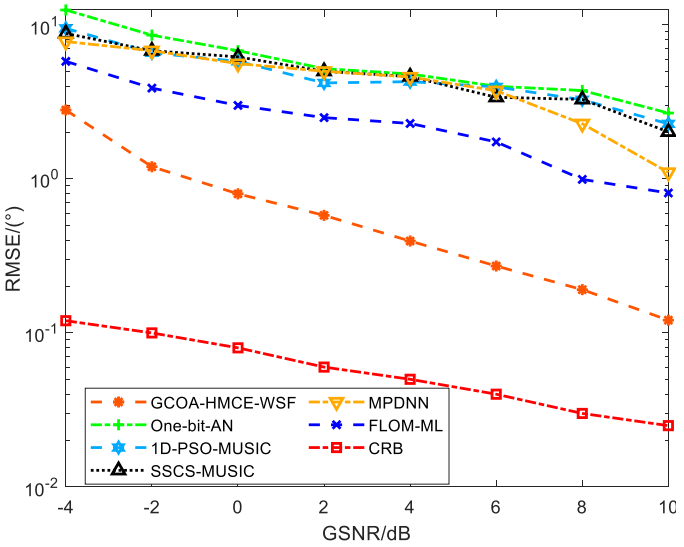

FIGURE 9. RMSE simulation curves of two coherent sources under different GSNRs.

5. CONCLUSION

Aiming at the problem of poor performance of traditional DOA estimation methods in an impulsive noise environment, this paper first introduces a new exponential kernel-hyperbolic tangent kernel. On this basis, the Toeplitz matrix is constructed by smoothing the spatial array and median filtering, and the covariance of the matrix is processed by the method of median deviation correntropy and hyperbolic tangent kernel, so as to effectively suppress impulse noise. Finally, the proposed GCOA algorithm is used to solve the weighted signal subspace fitting equation. The simulation results show that the GCOA-HMCE-WSF method proposed in this paper can effectively locate independent sources and coherent sources in complex impulsive noise environments. Under the condition of the large-scale antenna array, DOA estimation of a single snapshot source can be carried out quickly and effectively. The proposed GCOAHMCEWSF method can achieve better performance than some previous methods in the case of a single snapshot and strong impulsive noise, and the superiority and robustness of the GCOA-HMCE-WSF method are tested. In the subsequent research, we will design new de-impact processing methods and single-snapshot direction-finding methods to improve the effectiveness and real-time performance of DOA estimation in harsher noise environments and design more effective multi-objective quantum swarm intelligence optimization algorithms to solve more complex DOA estimation problems.

REFERENCES

[1] Huang, H., Q. Liu, H. C. So, and A. M. Zoubir, "Low-rank and row-sparse decomposition for joint DOA estimation and dis-

torted sensor detection," *IEEE Transactions on Aerospace and Electronic Systems*, Vol. 59, No. 4, 4763–4773, 2023.

[2] Wang, L., X. Hu, and H. Liu, "Advanced interference mitigation method based on joint direction of arrival estimation and adaptive beamforming for L-band digital aeronautical communication system," *Electronics*, Vol. 13, No. 8, 1600, 2024.

[3] Zhang, Y. D. and M. W. T. S. Chowdhury, "Direction-of-arrival estimation in closely distributed array exploiting mixed-precision covariance matrices," *Signal Processing*, Vol. 220, 109463, 2024.

[4] Li, G., "Moment independent uncertainty importance measure for stochastic systems based on Gaussian process," *Journal of Mathematical Chemistry*, Vol. 60, No. 8, 1610–1631, 2022.

[5] Caratelli, D., R. Sabbadini, and P. E. Ricci, "Approximating the moments of generalized gaussian distributions via Bell's polynomials," *Axioms*, Vol. 12, No. 2, 206, 2023.

[6] Liu, Y., H. Gao, M. S. Greco, and F. Gini, "Robust DOA estimation of incoherently distributed sources considering mixed circular and noncircular signals in impulsive noise," *IEEE Signal Processing Letters*, Vol. 31, 1900–1904, 2024.

[7] Liu, Y., H. Gao, Y. Du, M. Chen, and R. Sun, "DOA estimation for mixed circular and noncircular coherently distributed sources under impulsive noise," *IEEE Transactions on Aerospace and Electronic Systems*, Vol. 60, No. 5, 6622–6637, Oct. 2024.

[8] Liu, Y., H. Gao, M. Chen, A. Jakobsson, and J. Cheng, "A robust direction of arrival estimation method for coherently distributed sources in an impulsive noise environment," *IEEE Sensors Journal*, Vol. 23, No. 13, 14 375–14 387, Jul. 2023.

[9] Tanyildizi, E. and G. Demir, "Golden sine algorithm: A novel math-inspired algorithm," *Advances in Electrical & Computer Engineering*, Vol. 17, No. 2, 71, 2017.

[10] Du, P., J. Wang, Y. Hao, T. Niu, and W. Yang, "A novel hybrid model based on multi-objective Harris hawks optimization algorithm for daily PM2.5 and PM10 forecasting," *Applied Soft Computing*, Vol. 96, 106620, 2020.

[11] Tsakalides, P. and C. L. Nikias, "Maximum likelihood localization of sources in noise modeled as a stable process," *IEEE Transactions on Signal Processing*, Vol. 43, No. 11, 2700–2713, 1995.

[12] Dehghani, M., Z. Montazeri, E. Trojovská, and P. Trojovský, "Coati Optimization Algorithm: A new bio-inspired metaheuristic algorithm for solving optimization problems," *Knowledge-Based Systems*, Vol. 259, 110011, 2023.

[13] Meng, A.-B., Y.-C. Chen, H. Yin, and S.-Z. Chen, "Crisscross optimization algorithm and its application," *Knowledge-Based Systems*, Vol. 67, No. 4, 218–229, 2014.

[14] Wang, Z., D. Wang, B. Bai, *et al.*, "Direction finding algorithm of correlated interferometer based on genetic algorithm with high degree of stretching," *Systems Engineering and Electronics*, Vol. 40, No. 1, 39–44, 2018.

[15] Ge, S., C. Fan, J. Wang, and X. Huang, "Low-complexity one-bit DOA estimation for massive ULA with a single snapshot," *Remote Sensing*, Vol. 14, No. 14, 3436, 2022.

[16] Lakumalla, N. and P. K. Kumar, "Enhanced single-snapshot 1-D and 2-D DOA estimation using particle swarm optimization," *Traitement du Signal*, Vol. 40, No. 3, 1267–1273, 2023.

[17] Jia, T., H. Wang, and X. Shen, "A study of compressed sensing single-snapshot DOA estimation based on the RIPless theory," *Telecommunication Systems*, Vol. 74, No. 4, 531–537, 2020.

[18] Zhang, B., J. He, P. Liu, L. Wang, and R. Tang, "An automated multi-layer perceptron discriminative neural network based on Bayesian optimization achieves high-precision one-source single-snapshot direction-of-arrival estimation," *Scientific Reports*, Vol. 14, No. 1, 10300, 2024.

[19] Shao, M. and C. L. Nikias, "Signal processing with fractional lower order moments: Stable processes and their applications," *Proceedings of the IEEE*, Vol. 81, No. 7, 986–1010, 1993.